Monte Carlo simulation on aging processes within one `pure state' of the SK spin-glass model

1997 J. Phys. A: Math. Gen. 30 3891

(http://iopscience.iop.org/0305-4470/30/11/018)

J. Phys. A: Math. Gen. **30** (1997) 3891–3906. Printed in the UK PII: S0305-4470(97)80519-7

Monte Carlo simulation on aging processes within one 'pure state' of the SK spin-glass model

Hajime Takayama†, Hajime Yoshino‡ and Koji Hukushima§

Institute for Solid State Physics, The University of Tokyo, 7-22-1 Roppongi, Minato-ku, Tokyo 106, Japan

Received 12 December 1996, in final form 17 March 1997

Abstract. Monte Carlo simulations on the SK model have been done to investigate aging processes after a rapid quench from $T = \infty$ to the spin-glass phase. Taking care of time ranges of simulation, we examine time evolutions of energy of the system, Parisi's overlap distribution function, auto-correlation and clones-correlation functions, distribution functions of the two correlations, and magnetization induced by the field applied after a certain waiting time. The data simulated exhibit a rich variety of aging phenomena. Most of them can be interpreted in a unified way, though qualitatively, by the scenario of *growth of quasi-equilibrium domains* which we have recently introduced. The results are consistent qualitatively with asymptotic behaviours of some of the basic assumptions and their results in recent analytical theory on the same SK model, so long as the limiting procedures in finite systems are taken properly. Also they suggest that a basin of attraction of one dominant pure state spans almost an entire phase space of the system with a common time-reversal symmetry.

1. Introduction

Since the first observation by Lundgren *et al* [1] aging phenomena in spin glasses have been extensively studied [2]. They are expected to reveal the nature of the low-temperature spin-glass phase which has yet to be settled despite nearly two decades of dispute. One of the key concepts on aging phenomena recently introduced by Bouchaud [3] is the *weak-ergodicity breaking* (WEB). It was introduced during the argument on his trap model where many metastable states, or 'traps', exists. Depths of the traps are distributed continuously in such a way that the average time for the system to escape from them by thermal activation process is infinite; or, it takes an infinite time for the system to equilibriate. Subsequently the WEB picture has been incorporated in many works on aging phenomena in mean-field spin-glass models as well as in some related models [4–8]. These works have revealed that the WEB concept is much more general than initially proposed; it can be applied to aging phenomena in a system even without metastable states [9]. The WEB picture is now represented in terms of the double-time (spin) auto-correlation function $C(t, t') \equiv N^{-1} \sum_i S_i(t) S_i(t')$ as follows

$$\frac{\partial C(t,t')}{\partial t} \leqslant 0 \qquad \text{and} \qquad \frac{\partial C(t,t')}{\partial t'} \geqslant 0 \qquad (t \geqslant t') \tag{1a}$$

† E-mail address: takayama@issp.u-tokyo.ac.jp
‡ E-mail address: yhajime@ginnan.issp.u-tokyo.ac.jp
§ E-mail address: fukusima@ginnan.issp.u-tokyo.ac.jp

0305-4470/97/113891+16$19.50

$$\lim_{t-t'\to\infty}\lim_{t'\to\infty} C(t,t') = q_c \qquad (>0) \tag{1b}$$

$$\lim_{t\to\infty} C(t,t') = 0 \qquad \text{for a fixed } t'(<\infty) \tag{1c}$$

where q_c is a certain constant.

Various simulations which reproduce some aspects of the experimentally observed aging phenomena have already been reported [10–13]. But they are not yet satisfactory to be able to understand the phenomena in a unified way. Since the recent phenomenological and theoretical arguments mentioned above, as well as recent analyses on experiments [14, 15], are more or less based on the mean-field picture of spin glasses, we believe it is worth examining aging phenomena in the mean-field spin-glass model in more detail by simulations [16]. In the present work therefore we have performed Monte Carlo (MC) simulation on the SK model [17], whose equilibrium properties are well understood [18]. Its purpose is to obtain various information on its aging phenomena, including those which are related to the above-mentioned key concept.

The aging phenomena we are concerned with are non-equilibrium processes toward equilibrium observed in macroscopic systems in long but finite intervals of time. Since, on the other hand, the present simulations are performed only on finite systems with N spins, we have to take care of their time range. Suppose the system has a continuous distribution of relaxation times with the maximum $t_{\rm erg}^{\rm M}(N,T)$ which may depend also on temperature T, and whose systematic dependence on N is known. The WEB is expected to occur in such systems with $\lim_{N\to\infty} t_{\rm erg}^{\rm M}(N,T) = \infty$. Therefore simulations on finite systems have to be done in the time range of $t \lesssim t_{\rm erg}^{\rm M}(N,T)$ otherwise expected aging phenomena in the thermodynamic limit are obscured by processes with complete equilibration.

According to Parisi's picture [18] on the spin-glass phase of the SK model in equilibrium, there are many pure states which are separated from each other by insurmountable free-energy barriers. More explicitly, it was argued that in systems with large N two types of the free-energy barriers exist: one between the pure states with a common time-reversal symmetry, and the other between those with opposite time-reversal symmetries [19, 20]. The characteristic times, $t_{\rm erg}^{\rm S}(N,T)$ and $t_{\rm erg}^{\rm L}(N,T)$, needed to surmount respectively the former and latter barriers are given by (see figure 2)

$$\ln t_{\rm erg}^{\rm S}(N,T) \propto N^{1/4} \qquad \text{and} \qquad \ln t_{\rm erg}^{\rm L}(N,T) \propto N^{1/2}. \tag{2}$$

Therefore we have to set at least $t_{\rm erg}(N,T) \lesssim t_{\rm erg}^{\rm S}(N,T)$, $t_{\rm erg}(N,T)$ being the upper boundary of the time range after a rapid quench, where proper aging phenomena are observed in finite systems. In the present work we call such a limited time interval an *aging range*, and a portion of phase space that the system explores within that interval a *'pure state'*.

The fact that $t_{\rm erg}(N,T)$ is finite in finite systems makes it rather difficult to compare results of simulations on finite systems with the basic assumptions and their results in the theoretical arguments mentioned above. In the latter, for example in equations (1*b*, *c*), the limit $N\to\infty$ is taken before the limits t and/or $t'\to\infty$. One of the simplest ways to examine such limits by simulations is to examine them only through quantities which are independent of N. That is, however, practically hard to do. Instead, an efficient strategy is to analyse aging phenomena in finite systems in detail and to extrapolate the obtained (N-dependent) results to $N\to\infty$. By such analyses we will argue that $\lim_{t'\to\infty}\lim_{N\to\infty}$ in the theories corresponds to $\lim_{N\to\infty}\lim_{t'\to t_{\rm erg}(N,T)}$ in the simulation. We also emphasize that the study of aging phenomena in finite systems is of importance by itself since it may provide us with information on the 'interrupted aging' in some systems [3, 12].

In the present work we simulate time evolution of various quantities after the quench; energy of the system, Parisi's overlap distribution function, auto-correlation and clones-

correlation functions [16, 21, 22], and distribution functions of the two correlations. The magnetization induced by the field applied after a waiting time t_w is also investigated. It has turned out that the data simulated exhibit a rich variety of aging phenomena. They indicate complexity of the rugged free-energy landscape within the 'pure state'. It is expected to have many free-energy barriers of finite heights which are surmountable within the aging range introduced above. Most of our simulated results can be interpreted in a unified way, though qualitatively, by the scenario of *growth of quasi-equilibrium domains* (GQED) which we have recently introduced [23, 24].

In [24] we have solved numerically the master equation of the SK model but of small sizes ($N \leqslant 12$), and looked for time evolution of the probabilities of occurrence $p_\alpha(t; T)$ after rapid quench to a certain temperature T below T_c, where α specifies the TAP solutions at $T = 0$ (which we call here 'states'). It is found that the ratios, $r_\alpha(t; T) \equiv p_\alpha(t; T)/p_\alpha(\infty; T)$ with $p_\alpha(\infty; T)$ being the equilibrium Boltzmann weight, exhibit a tree structure when they are plotted against t; at a certain time $r_\alpha(t; T)$ a few states coincide with each other (or, leaves merge with a branch), at a later time a few such branches merge with a bigger branch, and finally all branches merge with a trunk ($r_\alpha(t; T) = 1$ for all α). This means that at and after the stage where a few states merge to a branch these states are in quasi-equilibrium in the sense that their relative weights coincide with those in equilibrium. We have called the portion of phase space associated with these states the quasi-equilibrium domain, and an aging process represented by the aforementioned tree the GQED process. One of the main purposes of the present work is to ascertain this GQED scenario in the SK model of larger sizes by MC simulation.

Besides the GQED scenario the present results suggest that the basin of attraction of one 'pure state' spans an almost entire phase space with a common time-reversal symmetry. We call this feature the *dynamic dominant pure-states picture*. In view of the equilibrium properties of the SK model, on the other hand, there is the argument [25] that among many pure states only a few (even one) of them dominate the Gibbs–Boltzmann measure. We call this aspect the *static dominant pure-states picture*. Our simulated data suggest that the properties inside the dynamic dominant pure state almost coincide with those of the static dominant pure state.

In the next section the model and method of our simulations are briefly explained. In section 3 we present the results of the simulations which are interpreted by our GQED scenario in section 4. In these sections the following notations are used for the double-time functions such as $C(t, t')$ in equations (1); $t = \tau + t_w$, and $t' = t_w$. The final section is devoted to the concluding remarks.

2. Model and method

By means of the standard heat-bath method of the MC simulation we have studied the $\pm J$ SK model with mean zero and variance $(N-1)^{-1/2}$ [26]. The system sizes examined are $N = 32$–2048, particularly $N = 128$, 512 in detail. The present work analyses mainly the aging processes after rapid quenches from $T = \infty$ to T below the spin-glass transition temperature T_c ($= 1$ in the limit $N \to \infty$). Simulation of this process is to simply perform a MC run at T starting from a random spin configuration. Physical quantities are obtained by taking the average over such M independent MC runs for each realization of $\{J_{ij}\}$ (sample) and over the N_s samples. Those at time t (in units of 1 MC step per spin) in each MC run

are evaluated by means of the following short time average,

$$A^{(m)}(t) = \frac{1}{\Delta t + 1} \sum_{t'=t-\Delta t}^{t} a^{(m)}(t') \tag{3}$$

where $a^{(m)}(t')$ is the value of quantity A at step t' of the mth MC run, and $\Delta t \ll t$ (for example $\Delta t = 0$ for $t < 16$ and 511 for $t \geqslant 2^{13}$). In the present work we put $M = 10$ and $N_s = 40$–2000 depending on N.

Most of our simulations are performed in the aging range mentioned in the previous section. Here we make a further comment on a cut-off of the aging range in the shorter side. The time range of simulations should not be too short in order to distinguish aging phenomena peculiar to spin glasses from certain initial transient processes expected to exist in any system. We denote a timescale of this short cut-off as $t_{\mathrm{q.e.}}$. Its explicit value, as well as that of $t_{\mathrm{erg}}(N, T)$ mentioned in section 1, will be discussed below referring to our simulated data.

3. Results

3.1. Energy and Parisi's overlap distribution

Let us first investigate the time evolution of the energy $E(t)$ after the quench at $t = 0$. As shown in figure 1(a), the energy per spin drops rapidly and then gradually saturates to the N-dependent equilibrium value E_{eq}/N. Interesting information is obtained when we look at how the extensive energy $E(t)$ approaches E_{eq}. In figure 1(b) we show $\Delta E(t) \equiv E(t) - E_{\mathrm{eq}}$ where E_{eq} is approximated by $E(t_{\max})$ with $t_{\max}$ being the (N-dependent) maximum t of the MC observation. The time $t^{\mathrm{E}}_{\mathrm{erg}}(N, T)$, defined by $\Delta E(t^{\mathrm{E}}_{\mathrm{erg}}) \cong T$, is shown in figure 2. It has the same N-dependence as that of $t^{\mathrm{S}}_{\mathrm{erg}}(N, T)$ of equation (2) obtained previously [19], although the proportional constants are different. In the present work we adopt $t^{\mathrm{E}}_{\mathrm{erg}}(N, T)$ as the upper boundary of the aging range, or $t_{\mathrm{erg}}(N, T) \simeq t^{\mathrm{E}}_{\mathrm{erg}}(N, T)$. In figure 1($c$) $\Delta E(t)/N$ versus t is plotted double logarithmically. The data of $N = 512$, 1024, and 2048 almost coincide with each other in the range $t \lesssim 2000$, indicating that slow decay in $\Delta E(t)/N (\propto t^{-\alpha}, \alpha \simeq 0.55)$ is a genuine property in the aging range of the system even with $N = \infty$. (The deviation of data of $N = 2048$ (diamonds) from the common curve at larger t is considered due to a poor estimate of E_{eq}.) Similar slow dynamics in $\Delta E(t)/N$ has been reported in other model systems [21, 27].

In figure 3 the time evolution of Parisi's overlap distribution functions $P(q; t)$ is demonstrated for systems with $N = 128$ at $T = 0.4$. Here q is one of $M(M-1)/2$ overlaps of magnetization configurations $q(t) = N^{-1} \sum_i m_i^{(k)}(t) m_i^{(l)}(t)$ where $m_i^{(k)}(t)$ is evaluated by equation (3) with $a = S_i$. In the figure the heavy broken curve represents $P_{\mathrm{RSB}}(q)$, i.e. $P(q)$ in equilibrium and in the thermodynamic limit which is evaluated by solving numerically Parisi's equation [28]. The position of its delta peaks are specified $\pm q_{\mathrm{EA}}$; the self-overlap parameter [18]. As already reported by Bhatt and Young [20], $P(q; t)$ evolves from a single Gaussian centred at $q = 0$ at $t = 0$ to a structure with double peaks (but of significant widths) similar to $P_{\mathrm{RSB}}(q)$ at large enough t. In the present analysis we determine $t^{\mathrm{L}}_{\mathrm{erg}}(N, T)$ as the time at which $P(q \simeq 0; t)$ converges to $P_{\mathrm{RSB}}(q \simeq 0)$ and we also show it in figure 2. We see in figure 3 that at $t = 512 \simeq t^{\mathrm{E}}_{\mathrm{erg}}(N = 128, T = 0.4)$, $P(q; t)$ already exhibits the double peaks around $q = \pm q_{\mathrm{EA}}$, though the peak position is shifted a little from q_{EA} due to the finite-size effect. It is also noted that the peak at $q \simeq 0$ still remains.

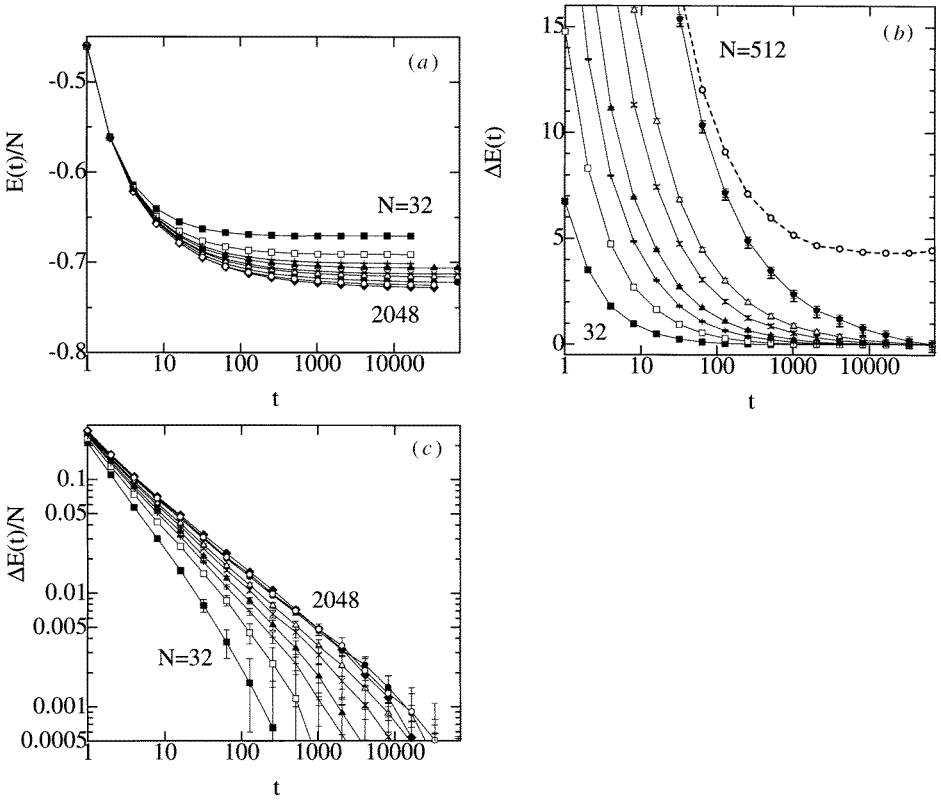

Figure 1. Time evolution of energy at $T = 0.4$. (a) Energy per spin in systems with $N(N_s)$ =32(2000), 64(2000), 96(2000), 128(1000), 192(600), 256(500), 512(200), 1024(40), and 2048(50) from top to bottom. (b) Extensive energy difference $E(t) - E_{eq}$ ($= \Delta E(t)$) for $N = 32$–512. The data shown with broken line represent $\Delta E(t) + E_B(t)$ for $N = 512$ (see text for definition of $E_B(t)$. (c) Double-logarithmic plot of $\Delta E(t)/N$ versus t_a. N and N_s are the same as in (a), but here from bottom to top.

3.2. Auto-correlation function

In figure 4(a) we show typical data of the auto-correlation function $C(\tau + t_w, t_w)$. It is obtained at $T = 0.4$ of systems with $N = 512$ in the range $t = \tau + t_w \lesssim 3 \times 10^4$. One can see that $C(\tau + t_w, t_w)$ satisfies equation (1a), i.e. one of the WEB conditions. Also the data exhibit crossover behaviour from relatively 'fast' decay in $\tau < t_w$ (except for initial, very rapid decay) to relatively 'slow' decay in $\tau > t_w$ (note that 'fast' and 'slow' here are the decay rates with respect to t, while those with respect to logarithms of t as seen in figure 4(a) appear oppositely). The behaviour is common to $C(\tau + t_w, t_w)$ simulated in various systems [10–12, 29], and is interpreted as a crossover from quasi-equilibrium to out-of-equilibrium behaviour.

An interesting feature becomes clear if we plot $C(\tau + t_w, t_w)$ against $\ln(\tau/t_w)$, as shown in figure 4(b). As first pointed out by Baldassarri [16], $C(\tau + t_w, t_w)$ with different t_w, except for $t_w = 2^{14}$, cross almost at a point $\tau \simeq t_{crs}$. This behaviour is certainly different from those of $C(\tau + t_w, t_w)$ observed in the previous works [11, 12, 29], whose $C(\tau + t_w, t_w)$ with different t_w's in the out-of-equilibrium range are rather well scaled to a single curve when plotted against τ/t_w. We also note that $\ln t_{crs} \simeq \ln t_w$ and that the value of $C(t_{crs} + t_w, t_w)$

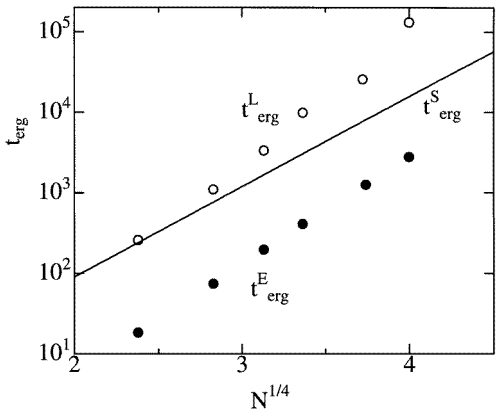

Figure 2. The system-size (N) dependence of characteristic relaxation times related to aging processes in the SK model at $T = 0.4$ for $N \leqslant 256$; $t^{\mathrm{L}}_{\mathrm{erg}}(N,T)$ and $t^{\mathrm{S}}_{\mathrm{erg}}(N,T)$ of equation (2) and $t^{\mathrm{E}}_{\mathrm{erg}}(N,T)$ determined by $\Delta E(t^{\mathrm{E}}_{\mathrm{erg}}) = 0.5$ $(= 1.2T)$ from figure 1(b). The full line is $\ln(t^{\mathrm{S}}_{\mathrm{erg}}(N,T)) = 2.56N^{1/4} - 0.66$ due to [19]. The area below $t^{\mathrm{E}}_{\mathrm{erg}}(N,T)$ $(\sim t_{\mathrm{erg}}(N,T))$ is the aging range introduced in the present work.

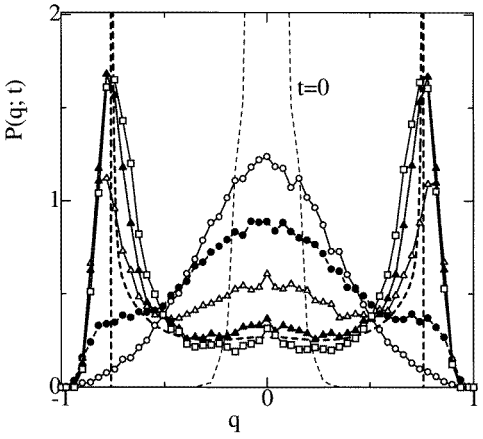

Figure 3. Parisi's overlap distribution function $P(q;t)$ for $N = 128$, $T = 0.4$. It is normalized as $\int_{-1}^{1} P(q;t)\,\mathrm{d}q = 1$. The data are t =16, 64, 512, 4096 and 32 768 from top to bottom at around $q \simeq 0$. The heavy broken curve represents $P_{\mathrm{RSB}}(q)$.

$(\simeq 0.62)$ is rather closer to $1 - T = \bar{q}$ $(= 0.6)$ than q_{EA} $(\cong 0.75)$, where $\bar{q} = \int_0^1 q(x)\,\mathrm{d}x$ is Parisi's order parameter in equilibrium [18].

We ascertain that the above crossing feature of $C(\tau + t_{\mathrm{w}}, t_{\mathrm{w}})$ is a genuine property of aging processes in the present system by the inspection of $C(t, t' = t/2)$ which can be simulated by a single aging process. As shown in figure 5 $C(t, t/2)$ for various N and T are nearly independent of t and N in the range $t_1 \lesssim t \lesssim t_2(N,T)$. Here $t_2(N,T)$ is a time around which $C(t, t/2)$ starts to decrease from its nearly constant value, and we have checked that it coincides with $t^{\mathrm{E}}_{\mathrm{erg}}(N,T)$ within logarithmic accuracy. On the other hand, the shorter timescale t_1 is regarded as $t_{\mathrm{q.e.}}$ (mentioned in section 2). The near constancy of $C(t, t/2)$ implies that $C(\tau + t_{\mathrm{w}}, t_{\mathrm{w}})$ with different t_{w}'s have a nearly common value at $\ln(\tau/t_{\mathrm{w}}) \simeq 0$.

Let us go back to figure 4(b) and discuss the deviation of the $t_{\mathrm{w}} = 2^{14}$ curve from the crossing behaviour. In fact it indicates that the system reaches equilibrium (but with time-reversal symmetry breaking) at this t_{w}; $C(\tau + t_{\mathrm{w}}, t_{\mathrm{w}})$ is now the function of only τ (time-translational invariant) so that, when plotted against $\ln(\tau/t_{\mathrm{w}})$, it shifts in parallel to the left. This feature is seen more clearly in $C(\tau + t_{\mathrm{w}}, t_{\mathrm{w}})$ in cases with smaller N and/or higher T within the range of our simulations. Since $C(\tau + t_{\mathrm{w}}, t_{\mathrm{w}})$ of $t_{\mathrm{w}} = 2^{13}$ with $N = 512$, $T = 0.4$ exhibits the crossing behaviour (not shown in figure 4(b)), we obtain $2^{13} \lesssim t_{\mathrm{erg}}(512, 0.4) \lesssim 2^{14}$, which is compatible with the specification $t_{\mathrm{erg}}(N,T) \simeq t^{\mathrm{E}}_{\mathrm{erg}}(N,T)$ in section 3.1.

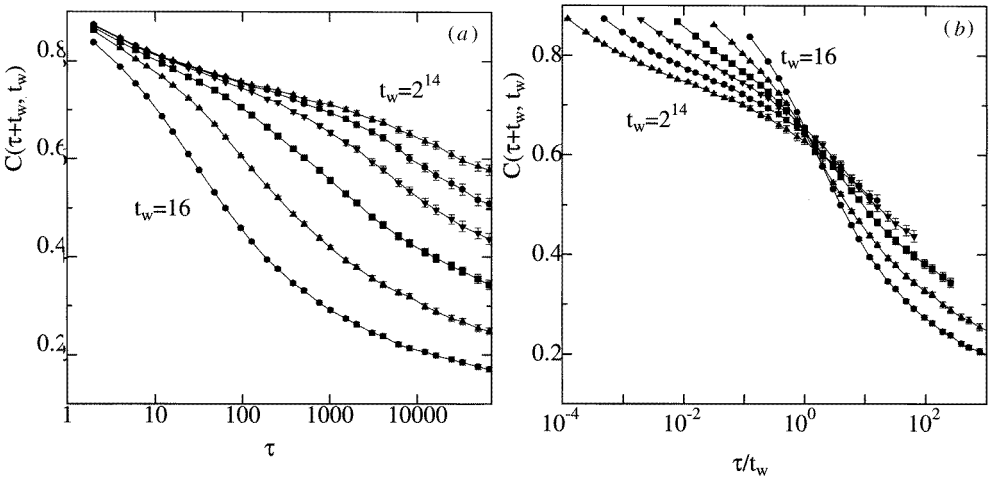

Figure 4. Auto-correlation functions $C(\tau + t_w, t_w)$ with $t_w = 2^{2n}$ ($n = 2$–7) plotted against t (a) and t/t_w (b) ($T = 0.4$, $N = 512$, $N_s = 100$).

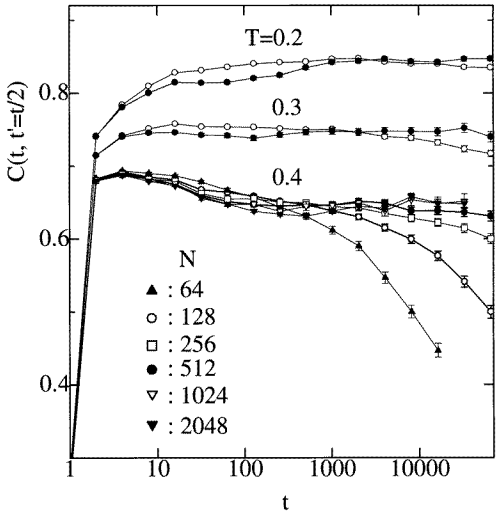

Figure 5. Auto-correlation functions $C(t, t/2)$ for some T and N.

3.3. Clones-correlation function

We have also investigated the clones-correlation function $Q(\tau + t_w, t_w)$ [16, 21, 22]. It is the correlation of two configurations starting from an identical one which has evolved up to $t = t_w$, but are evolving by means of two independent MC runs (with different sets of random numbers) at $t > t_w$. A typical result is shown in figure 6 for $T = 0.4$, $N = 512$. As found also by Baldassarri [16], $C(\tau + t_w, t_w)$ and $Q(\tau + t_w, t_w)$ cross at $\ln \tau \sim \ln t_w$. Their values at the crossing are again closer to $\bar{q}$ independently of t_w. A more remarkable feature seen in the figure is that as $\tau \to t_{erg}^{E}(N, T)$, $Q(\tau + t_w, t_w)$ with fixed t_w tend to saturate to constant values which depend on t_w. It is also noted (not shown) that $Q(\tau + t_w, t_w)$ plotted against $\ln(\tau/t_w)$ also cross nearly at a point similarly to $C(\tau + t_w, t_w)$ in figure 4(b).

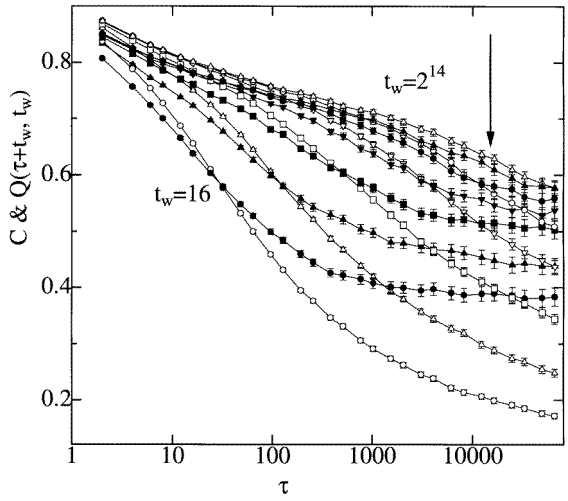

Figure 6. Clones-correlation functions $Q(\tau + t_w, t_w)$ with the same parameters t_w, T, N, N_s as in figure 4. Auto-correlation functions $C(\tau + t_w, t_w)$ are also shown by the lines with open symbols. The arrow indicates $t = t_{erg}(N, T)$.

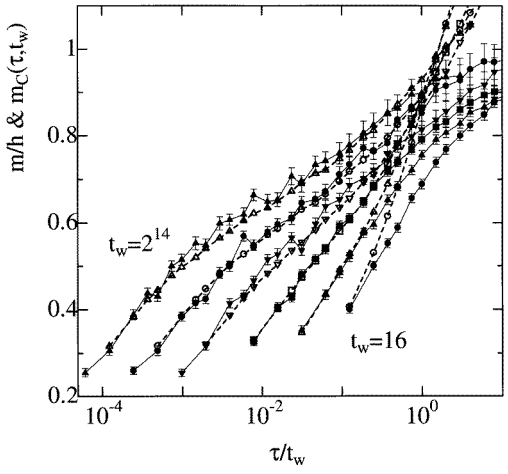

Figure 7. Induced magnetization $m(\tau; t_w)$ (symbols with full lines) and $m_C(\tau; t_w)$ (broken lines) of equation (4) with $t_w = 2^{2n}$ ($n = 2$–7) plotted against t/t_w ($T = 0.4$, $h = 0.04$, $N = 512$, $N_s = 100$).

3.4. Fluctuation-dissipation theorem

In order to get a further insight into aging processes we have simulated the magnetization $m(\tau; t_w)$ induced by the field h which is switched on at $t = t_w$. The result for $T = 0.4$, $N = 512$ and with $h = 0.04$ is drawn against $\ln(\tau/t_w)$ in figure 7. $m_C(\tau; t_w)$ are also shown by broken curves in the figure, defined by

$$m_C(t; t_w) = h\{1 - C(t + t_w, t_w)\}/T. \tag{4}$$

The fluctuation-dissipation theorem (FDT) tells us that, in equilibrium and for an infinitesimally small h, $m(\tau; t_w)$ and $m_C(\tau; t_w)$ are independent of t_w and $m(\tau) = m_C(\tau)$ holds. We see in figure 7 that, as observed in other model systems [10, 13, 29], $m(\tau; t_w) \cong m_C(\tau; t_w)$ holds in the time range $\tau \lesssim t_w$ with t_w larger than a certain value which corresponds to $t_{q.e.}$, the initial transient time mentioned in section 1.

4. Discussions

4.1. Scenario of growth of quasi-equilibrium domains

In order to interpret the above results of our simulations, let us first remind the reader of the following properties of the SK model in equilibrium. It is known that the TAP equation [31] of the SK model has a huge number of solutions in the spin-glass phase [32]. At $T = 0$ energies of one spin-flip stable states have a Gaussian distribution centred at $E/N \simeq 0.5$ with variance proportional to $N^{-(1/2)}$ [32, 33]. At finite temperatures it is pointed out that the TAP solutions lie just on the boundary of the validity condition of the TAP free-energy itself [34]. But neither further details of their stability nor their corresponding free-energy distribution have been well established. In the present argument, therefore, we call the solutions 'states' simply. In equilibrium only a very limited number of the states have significant probability weights $P_\alpha (\propto \exp(-F_\alpha/T))$ where F_α is the TAP free energy of the αth state [25] (the *static dominant pure-states picture* mentioned in section 1). Associated with such lowest free-energy states are limited portions of phase space which are separated by free-energy barriers described by equation (2). The aging processes simulated in the present work are interpreted to reflect the free-energy landscape of such local regions centred at each lowest free-energy state. We may identify these regions to the 'pure states' introduced in section 1.

Based on the above assumption we briefly explain our GQED scenario, introduced in section 1. Each 'pure state' contains a huge number of the TAP solutions (states), as schematically shown in figure 8. The lower their energies, the less the number of the states is. (In the present work we do not explicitly refer to entropy effects which have not been evaluated in the present simulation.) After the rapid quench (associated with the initial transient time $t_{\text{q.e.}}$) the system is found in one of the huge number of states with a relatively higher energy, from which it starts to look for lower and lower energy states either by thermal activation processes or possibly by finding one of the paths without free-energy barriers [9]. In this context let us introduce here an 'effective barrier energy' $E_{\text{B}}(t)$ simply by $E_{\text{B}}(t) \simeq T \ln t$: by this $E_{\text{B}}(t)$ we suppose processes yielding relaxation times of the order of $\exp(E_{\text{B}}(t)/T)$ without specifying their mechanism(s).

Let us then suppose that at time $t = t_{\text{w1}}$ the system reaches a certain state, say S_1 in figure 8. In a time interval of $t = t_{\text{w1}} + \tau$ with $\tau \ll t_{\text{w1}}$ the system is fluctuating in a local

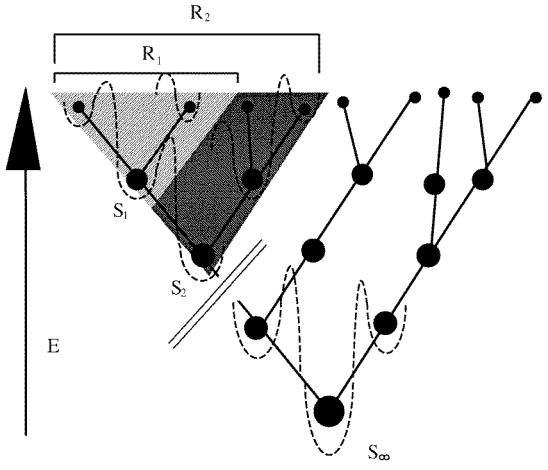

Figure 8. Schematic representation of the rugged energy structure of one 'pure state' of the SK model. The dots represent the TAP solutions (or states $S_1, S_2, \ldots, S_\infty$) and the shaded areas represent quasi-equilibrium domains ($R_1, R_2, \ldots$).

region R_1 centred at S_1 (the shaded area in figure 8), thereby it is expected to visit states in the region with frequencies according to their relative Boltzmann weights [24]. We call such regions R_1 *quasi-equilibrium domains*. As time goes on another interval of order t_{w1}, i.e. at $t = t_{w2} \simeq 2t_{w1}$, the system surmounts effective energy barrier $E_B(t_{w1})$ and finds a lower energy state, say S_2 in figure 8. This corresponds to entering into the out-of-equilibrium range of the waiting time t_{w1}. The state S_2 is, in turn, associated with the quasi-equilibrium domain R_2 of the waiting time t_{w2} which is larger than R_1. The quasi-equilibrium domain grows with time until it exhausts the whole 'pure state', or the system reaches the lowest energy state S_∞ in figure 8 (which takes an infinite time if $N = \infty$). This is our GQED scenario.

The GQED scenario explains straightforwardly the following results in the aging range obtained in the present MC study: (1) the monotonic decrease of the energy of the system ($\Delta E(t)$ in figures 1(*b*) and (*c*); (2) the crossover from quasi-equilibrium to out-of-equilibrium behaviour at around $\tau \sim t_w$ seen in $C(\tau + t_w, t_w)$ of figure 4; (3) the apparent FDT at $\tau \lesssim t_w$ demonstrated in figure 7, and (4) the behaviour of the clones-correlation shown in figure 6 which is explained as follows. Suppose the clones are created at $t = t_{w1}$ from a spin configuration near S_1 in figure 8. Then at $\tau \gtrsim t_{w1}$, the clones visit more frequently near the same state S_2 whose relative Boltzmann weight is largest in the larger domain R_2. The Hamming distance between them is then considered to be smaller than that between S_1 and S_2 which determines predominantly the value of the corresponding auto-correlation function. This means $Q(\tau + t_{w1}, t_{w1}) > C(\tau + t_{w1}, t_{w1})$ at $\tau \gtrsim t_{w1}$ as observed in the simulation.

Now let us go into further details of item (1). In figure 1(*b*) the value $\Delta E(t) + E_B(t)$ for $N = 512$ is also shown, where $E_B(t)$ is the effective energy barrier introduced above. From the figure we can extract the following two characteristic stages of the aging process; one is the early stage with $E_B(t) \ll \Delta E(t)$, and the other is the latest stage with $E_B(t) \gg \Delta E(t)$. The latter stage appears only in finite systems. The aging process in this stage is considered to be dominated by thermal-activated ones since $t^E_{erg}(N, T)$ itself roughly obeys the Arrhenius law: $\ln t^E_{erg}(N, T) \propto N^{1/4}/T$ (which will be reported separately elsewhere). Now let us introduce $t^F_{erg}(N, T)$, a crossover value above which the finite-size effects in aging phenomena become significant. One of its possible estimates is given by the condition $E_B(t^F_{erg}(N, T)) \simeq \Delta E(t^F_{erg}(N, T))$ and is about 1.5×10^3 for $T = 0.4$ and $N = 512$. At the moment we cannot specify definitely the aging process in the early stage (at $t_{q.e.} \lesssim t \lesssim t^F_{erg}(N, T)$), since we do not know details of the TAP solutions with relatively high energies as mentioned before. In this context we note that as seen in figure 1(*c*) the power-law behaviour of $\Delta E(t)/N$ seems to hold almost in the whole aging range, up to rather close to $t^E_{erg}(N, T)$, without any noticeable indication of the crossover around $t^F_{erg}(N, T)$. The same feature, i.e. aging phenomena exhibit no distinguishable difference in the aforementioned two stages, is seen also in $C(\tau + t_w, t_w)$ and $m_C(\tau; t_w)$ in figures 4(*b*) and 7, respectively. These results obtained within the accuracy of our simulation may indicate that either we have to put $t^F_{erg}(N, T) \simeq t_{erg}(N, T)$ (the finite-size effect appears almost suddenly just at $t_{erg}(N, T)$), mechanisms of relaxation processes are common in the two stages, or aging phenomena are insensitive to details of relaxation mechanisms. Which is the case is not clear at the moment. In any case, however, it is natural to interpret the limit $t' \to \infty$ in equation (1*b*) as corresponding to, in a finite system, the limit $t_w \to t_{erg}(N, T) (\simeq t^E_{erg}(N, T))$, at which the system is equilibrated as pointed out in figure 4(*b*).

The simulated results of items (2) and (3) have to be compared with equation (1*b*) and the

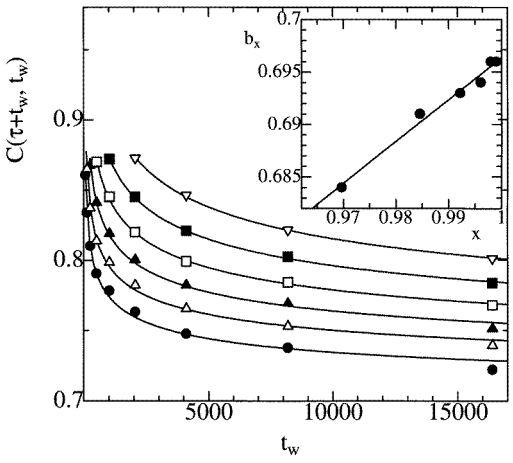

Figure 9. Autocorrelation function $C(\tau + t_{\rm w}, t_{\rm w})$ plotted against $t_{\rm w}$. The data points of the same symbols are those of the same $x \equiv t_{\rm w}/(\tau+t_{\rm w})$ but of various t and $t_{\rm w}$. The full curves represent the fitting curve for each data set of common x due to the empirical formula explained in the text. The value of x varies as $x = \frac{2^{11}}{2+2^{11}}, \frac{2^{10}}{2+2^{10}}, \ldots, \frac{2^{8}}{2+2^{8}}$ from the top to the bottom line. The inset shows the resultant fitting parameter b_x (see text) of various x together with a fitting line (full curve) which represents a linear fit of them.

recent arguments [5, 14] that both $C(\tau+t_{\rm w}, t_{\rm w})$ and $m(\tau; t_{\rm w})$ consist of two parts, equilibrium and aging ones, and that *in the limit* $t_{\rm w} \to \infty$ the FDT holds only for the equilibrium parts which depend on τ alone. Our data with the largest $t_{\rm w}$ $(= 2^{14} \gtrsim t_{\rm erg}(N, T))$ in figure 7 indicate that the FDT holds in the whole aging range $(\tau \lesssim t_{\rm erg}(N, T))$. Combined with our interpretation of the limit $t' \to \infty$ mentioned just above, this result is consistent with the argument in [5, 14]. Our data indicate further; the apparent FDT holds between the whole $C(\tau + t_{\rm w}, t_{\rm w})$ and $m(\tau; t_{\rm w})$ even for finite $t_{\rm w}(< t_{\rm erg}(N, T))$ for which $C(\tau + t_{\rm w}, t_{\rm w})$ depend not only on τ but also on $t_{\rm w}$ (see figure 4(*a*)). The latter means that the nature of overall fluctuation within each quasi-equilibrium domain differs between the domains and from true equilibrium. Still $C(\tau + t_{\rm w}, t_{\rm w})$ and $m(\tau; t_{\rm w})$ obey the apparent FDT. This is one of the main reasons why we propose the GQED scenario from the present MC analysis.

The check of the WEB condition of equation (1*b*) is further difficult since we need the extrapolation of $\tau \to \infty$ keeping the condition $\tau \ll t_{\rm w}$ $(\lesssim t_{\rm erg}(N, T))$. One of the ways to estimate $q_{\rm c}$ in equation (1*b*) is shown in figure 9, where we plot $C(\tau+t_{\rm w}, t_{\rm w})$ against $t_{\rm w}$. The data for a fixed $x \equiv t_{\rm w}/(\tau+t_{\rm w})$ are well fitted to an empirical form of $C_x(t_{\rm w}) = a_x t_{\rm w}^{-1/4} + b_x$ as shown by the full curves in the figures, where a_x, b_x are fitting parameters. In the inset of figure 9 we show $b_x = C_x(\infty)$ for various x. The value $\lim_{x\to 1} b_x \cong 0.70$ is an estimate for $q_{\rm c}$. It is considered to be a lower bound for $q_{\rm c}$, since $x \to 1$ implies the extrapolation of $t_{\rm w}$ far beyond the aging range. Although analysis here is only on $N = 512$, we consider this estimate to be compatible with the theoretical prediction of $q_{\rm c} = q_{\rm EA}$ [5]. It is also noted that this value is larger than $C(\tau + t_{\rm w}, t_{\rm w})$ at the crossing shown in figure 4(*b*).

4.2. Distribution functions of clone- and auto-correlations

The time evolution of distribution functions $P(Q; \tau, t_{\rm w})$ with $Q(\tau) = N^{-1} \sum_i m_i^{[1]}(\tau) m_i^{[2]}(\tau)$ shown in figure 10(*a*) further supports the scenario of the clones-correlation (item (4)). Here $m_i^{[k]}(\tau)$ is evaluated by equation (3) whose a on the r.h.s. is S_i of the kth clone. The distribution is therefore obtained from $MN_{\rm s}$ data points of $Q(\tau)$. A sharp peak of $P(Q; \tau, t_{\rm w})$ at $\tau \ll t_{\rm w}$ located around $Q \simeq q_{\rm EA}$ indicates simply that the clones are not yet separated enough and are fluctuating near the lowest energy state in the quasi-equilibrium domain of waiting time $t_{\rm w}$. Around $\tau \simeq t_{\rm w}$ the height of the peak decreases and its width increases. This is interpreted as the clones now tending to escape statistically independently of each other from the domain of $t_{\rm w}$. Interestingly, at $\tau = 2^{15} \gtrsim t_{\rm erg}(N, T) \gg t_{\rm w}$ the peak

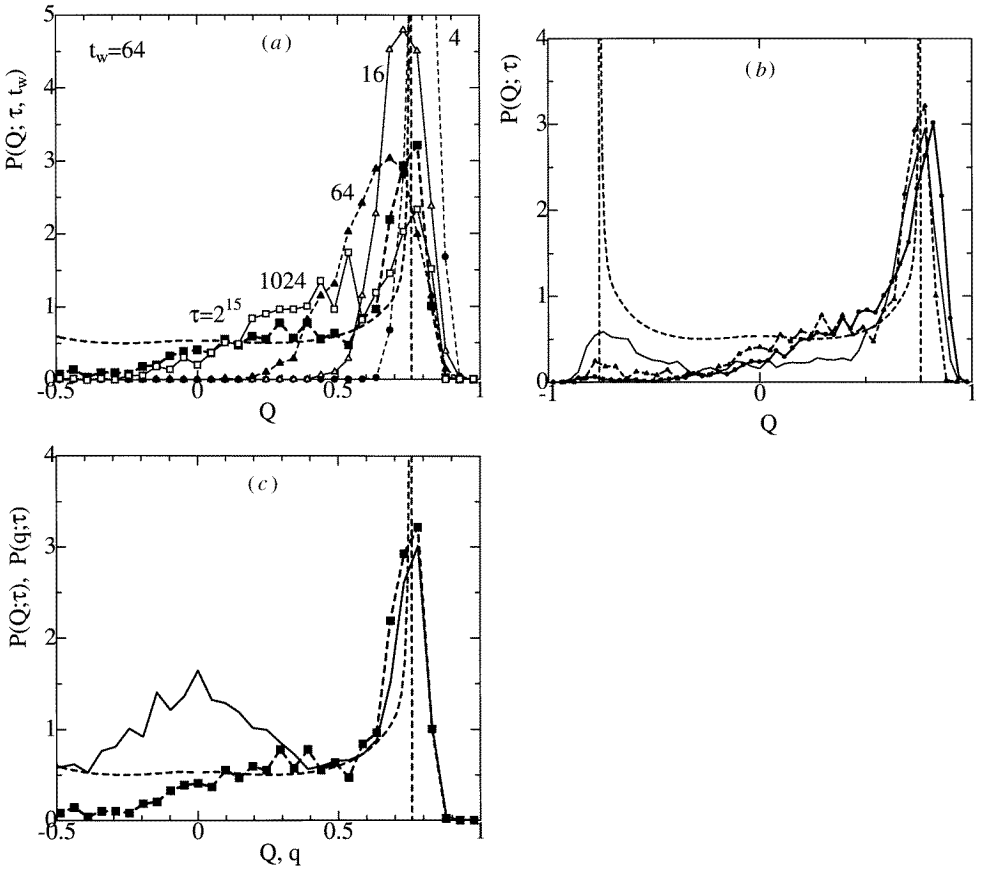

Figure 10. (*a*) Distribution functions of clones-correlation $P(Q;\tau,t_{\rm w})$ corresponding to the curve with $t_{\rm w}=64$ in figure 6. The broken curve without symbols represents $P_{\rm RSB}(q)$ (also in figures 10(*b*), (*c*), and 11). (*b*) Comparison of $P(Q;\tau,t_{\rm w})$ with $N=128$, 512 and $t_{\rm w}=64$: the full curve with circles represents $P(Q;\tau=512\simeq t_{\rm erg}^{\rm E},t_{\rm w})$ of $N=128$, the broken curve with triangles $P(Q;\tau=2^{15}\gtrsim t_{\rm erg},t_{\rm w})$ of $N=512$, and the light full curve $P(Q;\tau=2^{15}\simeq t_{\rm erg}^{\rm L},t_{\rm w})$ of $N=128$. (*c*) Comparison of $P(Q;\tau\sim t_{\rm erg},t_{\rm w})$ (broken curve with squares), $P(q;t\simeq t_{\rm erg})$ (full curve), and $P_{\rm RSB}(q)$ for $N=512$ and $T=0.4$. In this figure $P(q)$ are normalized as $\int_{-1}^{1}P(q)\,{\rm d}q=2$.

near $Q\simeq q_{\rm EA}$ sharpens again though its height does not recover very much. This result implies that in equilibrium at $\tau\gtrsim t_{\rm erg}(N,T)$ the clones reach the same lowest energy state with a large probability, and that $Q(\tau+t_{\rm w},t_{\rm w})$ for fixed $t_{\rm w}$ converge to certain finite values. The latter is in fact the case as we have already seen in figure 6; $Q(\tau+t_{\rm w},t_{\rm w})$ almost saturate to certain constants. Correspondingly, the shape of $P(Q;\tau,t_{\rm w})$ becomes a little dependent on τ at $\tau\gtrsim t_{\rm erg}(N,T)$).

In order to examine the N-dependence of the above characteristic feature in the clones-correlation, we show in figure 10(*b*) $P(Q;\tau,t_{\rm w})$ at $\tau\sim t_{\rm erg}(N,T)$ for $N=128$ and 512 both with $t_{\rm w}=64$. The two almost coincide with each other. The small difference in the peak positions near $Q=q_{\rm EA}$ is attributed to the finite-size effect. Naive extrapolation of these results to $N\to\infty$ is $\lim_{\tau\to\infty}Q(\tau+t_{\rm w},t_{\rm w})>0$ for a fixed $t_{\rm w}$ ($<\infty$). Thus the aging process within one 'pure state' of present interest belongs to type I by means of the

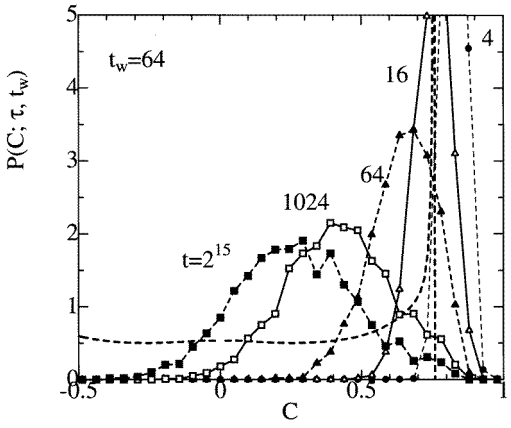

Figure 11. Distribution functions of auto-correlation $P(C;\tau,t_{\rm w})$ corresponding to the curve with $t_{\rm w}=64$ in figure 6. The curve without symbols represents $P_{\rm RSB}(q)$.

classification introduced by Barrat *et al* [22].

In figure 10(*b*) we also show, by the light full curve, $P(Q;\tau,t_{\rm w})$ at $\tau\simeq t_{\rm erg}^{\rm L}(N,T)$ for $N=128$. One sees that a small peak starts to develop not around $Q=0$ but around $Q=-q_{\rm EA}$. This result is interpreted as follow. When one of the clones surmounts the energy barrier between the phase spaces with different time-reversal symmetry, it goes down and situates itself near the counterpart of S_∞ within a time interval of $t_{\rm erg}(N,T)$ ($\ll t_{\rm erg}^{\rm L}(N,T)$).

In contrast to $Q(\tau+t_{\rm w},t_{\rm w})$ discussed above, $C(\tau+t_{\rm w},t_{\rm w})$ in figure 6 does not exhibit tendency of the saturation to certain finite values within the aging range of the present concern. Although it neither completely vanishes in the same time range, we expect that the weak-ergodicity breaking condition of equation (1*c*) holds in the limit $N\to\infty$ within its aging range. This expectation is derived from the inspection of the distribution functions of auto-correlation, $P(C;\tau,t_{\rm w})$ with $C(\tau)=N^{-1}\sum_i S_i(\tau+t_{\rm w})S_i(t_{\rm w})$, shown in figure 11. At $\tau>t_{\rm w}$, in contrast to $P(Q;\tau,t_{\rm w})$, $P(C;\tau,t_{\rm w})$ tends to become a Gaussian form whose centre tends to approach $C=0$. We therefore consider that equation (1*c*) holds since any configuration at $t'=t_{\rm w}$ ($<\infty$) in a 'pure state' is orthogonal to (separated far away from) the configuration at $t=\infty$, i.e. the lowest energy state of the 'pure state'.

According to Barrat *et al* [22], the above aging process of type I judging from $Q(\tau+t_{\rm w},t_{\rm w})$ and with the WEB judging from $C(\tau+t_{\rm w},t_{\rm w})$, is expected to appear, for example, in a system having a 'gutter' in phase space. But our GQED scenario is also compatible with the two characteristics. We only need a quite natural assumption that a basin of attraction of a 'pure state' is infinitely large if $N=\infty$. In fact our scenario is more appropriate judging from the time evolution of $P(Q;\tau,t_{\rm w})$ already described above. We may say that the energy structure in one 'pure state' is, instead of a 'gutter', a 'funnel' with an infinitely wide input mouth.

4.3. Dominant pure-states pictures

Finally, let us compare the three distribution functions $P(Q;\tau\sim t_{\rm erg},t_{\rm w})$, $P(q;t\simeq t_{\rm erg})$ and $P_{\rm RSB}(q)$ drawn in figure 10(*c*). Here $P(q;t\simeq t_{\rm erg})$ and $P_{\rm RSB}(q)$ (also those in figures 10(*a*)) and (*b*) are normalized as $\int_{-1}^{1}P(q)\,{\rm d}q=2$, differently from those in figure 3. The reason for this normalization is that time evolution of the clones at $\tau\sim t_{\rm erg}(N,T)$ ($\ll t_{\rm erg}^{\rm L}(N,T)$) of present interest is almost confined in a part of phase space with a common time-reversal symmetry, i.e. it is in equilibrium with time-reversal symmetry breaking. (A small weight

of $P(Q;\tau,t_w)$ smearing out to $Q<0$ is considered due to the finite-size effect.) It is rather surprising that near coincidence, $P(Q;\tau\sim t_{erg},t_w)\simeq P(q;t\simeq t_{erg}(N,T))\simeq P_{RSB}(q)$, holds for $Q,q\gtrsim 0.3$. (To be more accurate, near equality $P(q;t)\cong P_{RSB}(q)$ for all q is obtained only at t larger than $t^{L}_{erg}(N,T)$ as seen in figure 3 and in the previous work [20]. By 'near coincidence' here we disregard a quantitative difference in the weights associated with the peak at $Q,q\simeq q_{EA}$ as well as a qualitative difference in the shapes at $Q,q\lesssim 0.3$.)

The near coincidence $P(Q;\tau\sim t_{erg},t_w)\simeq P_{RSB}(q)$ alone indicates that the organization of states in one 'pure state' centred at the lowest energy state (S_∞ in figure 8) is similar to that of the whole phase space with a common time-reversal symmetry which gives rise to $P_{RSB}(q)$. The other near coincidence $P(Q;\tau\sim t_{erg},t_w)\simeq P(q;t\simeq t_{erg})$ tells us more since its r.h.s. quantity is the overlap between two configurations which start from random initial configurations independently chosen. Its plausible interpretation that we can think of is that a basin of attraction of one 'pure state' reached by our simulation in fact covers almost an entire phase space with a common time-reversal symmetry. This is what we have called the dynamic dominant pure-states picture in section 1. The near coincidence of the three distribution functions indicates that the free-energy landscape searched by the present simulation at around $t,\tau\sim t_{erg}(N,T)$ nearly coincides with that in equilibrium which is described by the static dominant pure-states picture [25]. In other words, it is a direct confirmation of the latter picture by means of the straightforward MC simulation. It is also noted that the argument here is for the time range of $t,\tau\sim t_{erg}(N,T)$, which may not directly correspond to the recent arguments on the analogous similarity between dynamic (aging) properties in the whole aging range and static ones [5, 35].

5. Conclusion

We have proposed the scenario that aging processes at a fixed T in the SK model, which are observed in the aging range of $t_{q.e.}\lesssim t\lesssim t_{erg}(N,T)$, are growth processes of quasi-equilibrium domains, or stochastic dynamics of the system looking for lower and lower energy states, and finally for dominant pure states which exhaust the probability weights in equilibrium. It qualitatively explains most of our simulated results. In our arguments extensive energies of states (solutions of the TAP equation), which are represented schematically by the ordinate of figure 8, and which govern relative Boltzmann weights in each quasi-equilibrium domain, play a central role. If, however, we want to know more details on the aging phenomena, such as an explicit functional form of $C(\tau+t_w,t_w)$, we have to analyse the organization of the states in the direction of the abscissa of figure 8.

We have also argued that there are the following five time ranges in relation to aging phenomena in the SK model of finite sizes: the initial transient range—$t_{q.e.}$—the early stage of the aging range—$t^{F}_{erg}(N,T)$—the latest stage of the aging range—$t_{erg}(N,T)$—the equilibrium range with time-reversal symmetry breaking—$t^{L}_{erg}(N,T)$—completely equilibrated range, where t denotes a crossover time between the corresponding two time ranges. At $\tau\gtrsim t_{erg}(N,T)$ the time-translational invariance in $C(\tau+t_w,t_w)$ is ascertained. It is then natural to consider that the limiting procedure $\lim_{N\to\infty}\lim_{t'\to t_{erg}(N,T)}$ in the present simulation corresponds to the one $\lim_{t'\to\infty}\lim_{N\to\infty}$ in the recent analytical theories. In fact by this interpretation the present results are consistent qualitatively with asymptotic behaviour of some of the basic assumptions and their results in the latter [5]. A further interesting observation is that the apparent FDT, as shown in figure 7, holds even for finite t_w ($<t_{erg}(N,T)$), although in the limited range of τ. It is considered important in analyses of actual experimental results, whose t_w (or t') by no means reaches to the literal

asymptotic limit $t' \to \infty$ by our above interpretation.

The two stages of the aging range are the early one specified by the condition $E_B(t) \ll \Delta E(t)$ and the latest one by $E_B(t) \gg \Delta E(t)$, where $E_B(t)$ and $\Delta E(t)$ are the effective barrier energy and the extensive energy relative to the equilibrium value, respectively. This division has been introduced expecting that in the latest stage aging phenomena affect by the finite-size effect and dominated by thermal activated processes are seen. Within the accuracy of the present analysis, however, no significant differences have been found in aging phenomena in the two stages (figures 1(*c*), 4, 6, and 7). It means that the nature of aging processes in the early stage, occurring through higher energy states whose Boltzmann weights in equilibrium are negligibly small, is not significantly different from that in the latest stage, occurring within the lowest energy states which nearly reproduce Parisi's overlap function in equilibrium. It may be related to the similarity between dynamic (aging) properties and static ones pointed out by the recent analytical theories [5, 35]. This problem is certainly one of the most challenging problems to be investigated further.

Acknowledgments

We are especially indebted to R Orbach and Y G Joh since this work was initiated from discussions with them on their experimental findings. We are grateful to J-P Bouchaud, L F Cugliandolo and J Kurchan for many stimulating discussions. We also acknowledge useful discussions with J Hammann, K Nemoto, P Nordblad, M Ocio, E Vincent and A P Young. The computation in this work was done using FACOM VPP500 of the Supercomputer Center, Institute for Solid State Physics, University of Tokyo. HY was supported by Fellowships of the Japan Society for the Promotion of Science for Japanese Junior Scientists. This work was supported by a Grant-in-Aid for International Scientific Research, 'Aging Phenomena in Complex Systems' (#08044060), and by a Grant-in-Aid for Scientific Research (#08640477), both from the Ministry of Education, Science and Culture, Japan.

References

[1] Lundgren L, Svedlindh P, Nordblad P and Beckman O 1983 *Phys. Rev. Lett.* **51** 911
[2] Vincent E, Hammann J and Ocio M 1992 *Recent Progress in Random Magnets* ed D H Ryan (Singapore: World Scientific) and references therein
[3] Bouchaud J-P 1992 *J. Physique* I **2** 1705
[4] Cugliandolo L F and Kurchan J 1993 *Phys. Rev. Lett.* **71** 173
[5] Cugliandolo L F and Kurchan J 1994 *J. Phys. A: Math. Gen.* **27** 5749
[6] Franz S and Mézard M 1994 *Physica* A **210** 48
[7] Bouchaud J-P and Dean D S 1995 *J. Physique* **5** 265
[8] Cugliandolo L F and Kurchan J 1995 *Phil. Mag.* **71** 501
[9] Kurchan J and Laloux L 1996 *J. Phys. A: Math. Gen.* **29** 1929
[10] Andersson J-O, Mattsson J and Svedlindh P 1992 *Phys. Rev.* B **46** 8297
Andersson J-O, Mattsson J and Svedlindh P 1994 *Phys. Rev.* B **49** 1120
[11] Cugliandolo L F, Kurchan J and Ritort F 1994 *Phys. Rev.* B **49** 6331
[12] Rieger H 1995 *Annual Review of Computational Physics* vol II, ed D Stauffer (Singapore: World Scientific)
[13] Franz S and Rieger H 1995 *J. Stat. Phys.* **79** 749
[14] Vincent E, Hammann J, Ocio M, Bouchaud J-B and Cugliandolo L F 1996 *Preprint* cond-mat/9607224
[15] Joh Y G, Orbach R and Hammann J *Preprint*
[16] Baldassarri A 1996 *Preprint* cond-mat/9607162
[17] Sherrington D and Kirkpatrick S 1975 *Phys. Rev. Lett.* **35** 1792
[18] Mézard M, Parisi G and Virasoro M A 1986 *Spin Glass Theory and Beyond* (Singapore: World Scientific)
[19] Mackenzie N D and Young A P 1982 *Phys. Rev. Lett.* **49** 301

[20] Bhatt R N and Young A P 1988 *J. Phys. C: Solid State Phys.* **21** L57
[21] Cugliandolo L F and Dean D S 1995 *J. Phys. A: Math. Gen.* **28** 4213
[22] Barrat A, Burioni R and Mézard M 1996 *J. Phys. A: Math. Gen.* **29** 1311
[23] Yoshino H 1997 *J. Phys. A: Math. Gen.* **30** 1143
[24] Yoshino H, Hukushima K and Takayama H 1997 *Prog. Theor. Phys. Suppl.* **126** to appear
[25] Mézard M, Parisi G, Sourlas N, Toulouse G and Virasoro M 1984 *J. Physique* **45** 843
[26] Picco M and Ritort F 1994 *J. Physique* I **4** 1619
[27] Barrat A 1997 *Preprint* cond-mat/9701021
[28] Nemoto K 1987 *J. Phys. C: Solid State Phys.* **20** 1325
[29] Yoshino H 1996 *J. Phys. A: Math. Gen.* **29** 1421
[30] Franz S and Rieger H 1995 *J. Stat. Phys.* **79** 749
[31] Thouless D J, Anderson P W and Palmer R 1977 *Phil. Mag.* **35** 593
[32] Bray A J and Moore M A 1980 *J. Phys. C: Solid State Phys.* **13** L469
[33] Nemoto K 1988 *J. Phys. A: Math. Gen.* **21** L287
[34] Nemoto K and Takayama H 1985 *J. Phys. C: Solid State Phys.* . **18** L529
[35] Baldssarri A, Cugliandolo L F, Kurchan J and Parisi G 1995 *J. Phys. A: Math. Gen.* **28** 1831